Available online at www.sciencedirect.com
SCIENCE DIRECT®
Journal of Molecular Catalysis A: Chemical 218 (2004) 253–259
JOURNAL OF MOLECULAR CATALYSIS A: CHEMICAL
www.elsevier.com/locate/molcata

Characterization and reactivity of silica-supported bimetallic molybdenum and stannic oxides for the transesterification of dimethyl oxalate with phenol

Xinbin Ma*,[1], Jinlong Gong[1], Shengping Wang, Fei He, Xia Yang, Gang Wang, Genhui Xu

Key Laboratory for Green Chemical Technology, School of Chemical Engineering and Technology, Tianjin University, Tianjin 300072, China

Received 2 October 2003; received in revised form 21 April 2004; accepted 21 April 2004

Abstract

A series of bimetallic MoO_3-SnO_2/SiO_2 catalysts with various Mo and Sn contents ranging from 1–16 wt.% were prepared by sequential impregnation with molybdate species and cationic Sn complexes using the wet impregnation method. The performance of these catalysts in the transesterification of dimethyl oxalate (DMO) with phenol was compared with corresponding stannum- and molybdenum-supported catalysts prepared by the same method. The results indicated that the catalyst of MoO_3-SnO_2/SiO_2 with 14 wt.% Mo and Sn contents performed best, giving 74.6% conversion of DMO and 99.5% selectivity to target products, methyl phenyl oxalate (MPO) and diphenyl oxalate (DPO). The component, structure and phase of MoO_3-SnO_2/SiO_2 catalysts with various Mo and Sn contents were investigated by means of X-ray diffraction (XRD), X-ray photoelectron spectroscopy (XPS), BET specific surface area measurement, temperature-programmed desorption of ammonia (NH_3-TPD), and FT-IR analysis of adsorbed pyridine. It was observed that interdispersion between MoO_3 and SnO_2 plays an important role in modifying the catalytic behavior. NH_3-TPD and FT-IR analysis of adsorbed pyridine results showed that only weak Lewis acids were present on the catalyst surface and the amounts of Mo and Sn loadings has hardly effected the strength of the surface acid. The weak Lewis acid sites catalyzed transesterification of DMO with phenol and Sn gave a promotional effect.

Keywords: Diphenyl carbonate; Diphenyl oxalate; Methyl phenyl oxalate; Transesterification; Dimethyl oxalate; Bimetallic MoO_3-SnO_2/SiO_2 catalysts; Lewis acid; Promotional effect

1. Introduction

Polycarbonate has been conventionally produced by the interfacial polycondensation of bisphenol-A (BPA) and phosgene. One of the major drawbacks of the conventional phosgene process is an environmental and safety problem involved in using copious amounts of methylene chloride as the solvent, which is ten times as much as the products on a weight basis, and highly toxic phosgene as the reagent [1]. However, phosgene-free processes for polycarbonate synthesis have been proposed that employ melt transesterification [2–5] or solid-state polymerization [1] using bisphenol-A and diphenyl carbonate (DPC) with the latter synthesized in a phosgene-free process.

Diphenyl carbonate has come to occupy an important position as useful organic chemicals for a variety of industrial and synthetic applications [6]. The industrial method employed commonly for synthesis of DPC is based on the reaction between phenol and phosgene in the presence of bases [6–9]. Because the current trend in the chemical industry is to reduce the risks connected with the use of highly toxic substances such as phosgene [10], alternative approaches to diphenyl carbonate production are either the interchange reaction of phenol with dimethyl carbonate (DMC) or dimethyl oxalate (DMO) and the oxidative carbonylation of phenol [11–18].

Among them, the transesterification of DMO with phenol via a three-step reaction has been deemed as a promising and possible route for DPC synthesis from the raw materials such as carbon monoxide, phenol and oxygen [19,20] (Eq. (1)). In the first step, dimethyl oxalate is produced by carbonylation of methanol [21]; then, diphenyl oxalate (DPO) is obtained from transesterification of DMO with phenol; and finally, the

* Corresponding author. Tel.: +86-22-27406498; fax: +86-22-27890905.
E-mail address: xbma@tju.edu.cn (X. Ma).
[1] These authors contributed equally to this work.

1381-1169/$ – see front matter © 2004 Elsevier B.V. All rights reserved.
doi:10.1016/j.molcata.2004.04.022

decarbonylation of DPO occur to produce DPC and carbon monoxide [22].

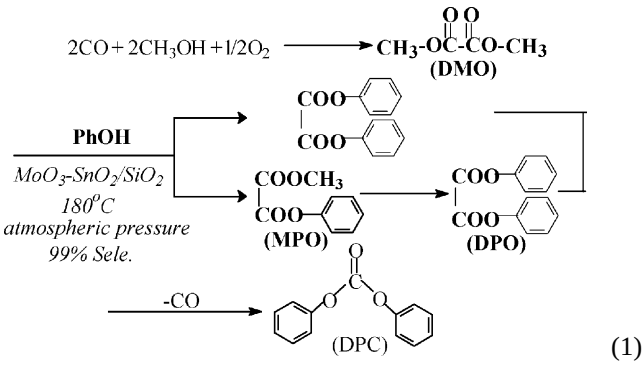

(1)

It is pointed that the synthesis of diphenyl oxalate (DPO) follows the two-step reaction module consisting of transesterification of DMO with phenol into methyl phenyl oxalate (MPO) and further transesterification or disproportionation of MPO into DPO, Eqs. (2)–(4).

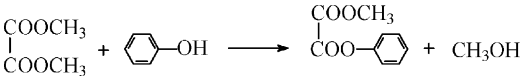

(2)

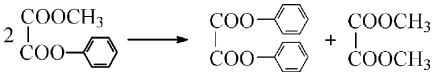

(3)

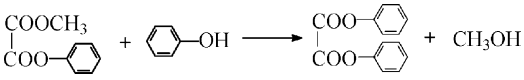

(4)

The thermodynamic equilibrium constants of reactions (2), (3) and (4) at 453 K are estimated at 0.23, 4.77×10^{-8}, and 2.09×10^{-7} [23], respectively, from the thermodynamic calculation made with group contribution of liquid components. This indicates that the transesterification between DMO and phenol, especially a further transesterification of MPO with phenol and the disproportionation of MPO are not favorable in the thermodynamics.

Nishihira et al. [19,20,22] reported the transesterification of DMO with phenol carried out in the liquid phase using traditional transesterification catalysts such as Lewis acids and soluble organic Pb, Sn, or Ti compounds. In these homogeneous systems, the separation and recovery of the catalysts remains a critical issue when applied to the industrial process. Therefore, the development of active solid catalysts is highly desirable in view of regeneration and separation. Unfortunately, there are few reports on the development of active heterogeneous catalysts for the reaction up to present time. Thus, the goal of our work was to develop a heterogeneous catalytic system that combines good catalytic performance and satisfactory recovery of the catalysts used.

During the last decade, a great deal of fundamental and applied researches were focused on supported molybdenum catalysts because of their multitudinous industrially important reactions including ammoxidation, selective oxidation [24–27], as well as petroleum refining and pollution control industries [28]. But it is also well-known that, in several reactions, catalysts based on multicomponent oxides exhibit better performance than separate component oxides. This has been accounted for in the literature by means of mechanisms such as "Remote Control" by spill over species [29] as well as by means of physico-chemical characterizations.

Various supported bimetallic molybdenum oxide catalysts have been synthesized and used. But for the transesterification of DMO with phenol, only the MoO_3/SiO_2 catalyst was tested [30]. Thus, we tried to develop a highly active catalyst for MPO and DPO synthesis that was based on silica-supported molybdenum oxide. Now, we find that silica-supported bimetallic molybdenum and stannic oxide is an excellent solid catalyst for the transesterification of DMO with phenol.

Therefore, as a continuation of previous studies, this paper will report the preparation, characterization and evaluation in the transesterification reaction of DMO with phenol over MoO_3-SnO_2 catalysts supported on silica.

2. Experimental

2.1. Catalysts preparation

Commercial silica was used as the support. Prior to impregnation it was dried at 393 K for 2 h. This treatment results in silica with a surface area of 231 m^2/g and average pore size of 80 Å, as measured with nitrogen adsorption.

The monometallic Mo, Sn and the bimetallic Mo-Sn catalysts were prepared by impregnation or sequential impregnation of 20 g of supports with $(NH_4)_6Mo_7O_{24}{\cdot}H_2O$ and $C_{32}H_{64}O_4Sn$ (dibutyltin dilaurate) using the conventional wet impregnation technique. The route of preparation using cationic Sn complex and Mo compounds was explored by Halasz and co-workers who concluded that a strong bimetallic interaction was obtained [31].

MoO_3/SiO_2 was prepared by dissolving $(NH_4)_6Mo_7O_{24}{\cdot}4H_2O$ in distilled water. After evaporation of the solvent at 353 K and reduced pressure, the solid obtained was dried at 393 K overnight and then, calcined in a muffle furnace at 823 K for 4 h.

SnO_2/SiO_2 was prepared by dissolving $C_{32}H_{64}O_4Sn$ in toluene at room temperature. After 18 h, the sample was dried at 393 K overnight and then calcined in a muffle furnace at 823 K for 4 h.

The bimetallic MoO_3-SnO_2/SiO_2 catalysts were prepared using a two-step procedure. The metals were impregnated in sequence. The first step involves a solvent impregnation of $(NH_4)_6Mo_7O_{24}{\cdot}4H_2O$ on pretreated SiO_2. The sample is vacuum-dried and calcined at 823 K for 4 h. On this MoO_3/SiO_2 material, $C_{32}H_{64}O_4Sn$ in toluene is loaded at room temperature and the resultant catalyst was dried under vacuum and then calcined in a muffle furnace at 823 K for 4 h. The catalyst is named MoO_3-SnO_2/SiO_2. A Mo/Sn ratio of 1.0 was chosen after a series of batch tests (carried out at

different Mo:Sn values) that have shown a typical volcano profile with the highest catalytic performance at Mo/Sn ratios around 0.9–1.1 [32].

2.2. Characterization techniques

2.2.1. Surface area

The specific surface areas (S_{BET}, m^2/g) of all samples were determined on a constant volume adsorption apparatus (CHEMBET-3000) by the N_2 BET method at the liquid nitrogen temperature.

2.2.2. X-ray diffraction (XRD)

X-ray powder diffraction patterns were recorded on a Rigaku C/max-2500 diffractometer using graphite filtered Cu Kα radiation ($\lambda = 1.5405$ Å) at 40 kV and 100 mA with a scanning rate of $8^\circ\,min^{-1}$ from $2\theta = 5^\circ$ to $2\theta = 80^\circ$. The XRD phases present in the samples were identified with the help of JCPDS Powder Data Files.

2.2.3. IR studies

The IR spectroscopic measurements of adsorbed pyridine were carried out on a Bruker VECTOR22 FT-IR spectrometer with $4\,cm^{-1}$ resolution in the 500–4000 cm^{-1} scanning range. The samples were pressed into $10\,mg/cm^2$ self-supporting wafers. Prior to each experiment, the catalysts were evacuated (1 Pa) at 693 K for 1.5 h. Then they were exposed to 303 K for 2 h. Following this, the material was exposed to 30 Torr of pyridine for 30 min, and finally evacuated for additional 1 h at 473 K. After adsorption, the samples were out-gassed and the spectra were recorded at room temperature. The treatments were carried out using a quartz IR cell [33].

2.2.4. X-ray photoelectron spectroscopy (XPS)

The surface composition and structure of catalyst were studied by X-ray photoelectron spectroscopy (XPS) in a Perkin-Elmer PHI 1600 ESCA system with Mg Kα 1253.6 eV radiation as the excitation source. The samples were mounted on a specimen holder by means of double-sided adhesive tape. Spectra were recorded in steps of 0.15 eV. The C1s peak (284.5 eV) was used as the internal standard for binding-energy calibration. An estimated error of ±0.1 eV can be assumed for all the measurements. The scanning of the spectra was done at pressures less than 10^{-8} Torr and the temperature was approximately 293 K.

2.2.5. Temperature-programmed desorption of ammonia (NH_3-TPD)

NH_3-TPD experiments were conducted on an Auto-chem 2910 (Micromeritics, USA) instrument. About 100 mg of the oven-dried sample was taken in a U-shaped quartz sample tube and the sample was pretreated in ultra high pure Ar (50 ml/min) at 393 K for 1 h and then cooled to ambient temperature. The pulses of ammonia were supplied to the samples to be saturated. Ammonia was replaced with argon and sample was heated to 873 K at a rate of 10 K/min.

2.3. Catalytic test

The reaction was conducted in a 250 ml glass flask equipped with a thermometer, a distillation apparatus, and a stirrer under refluxing condition at atmospheric pressure. Especially, the top of distillation column was kept at 353 K by flowing through recycled water in order to remove methanol from the reaction system. Thus, the reaction equilibrium limitation in reaction (2) was broken and the reaction was accelerated towards the desired direction. The reaction mixture contained 0.1 mol DMO, 0.5 mol phenol, and the catalyst. After the raw materials and the catalyst were placed into the batch reactor, nitrogen gas was flowed at $30\,cm^3$/min to purge the air from the reaction system. After 10 min, the nitrogen flow was stopped and the flask was heated at a rate of 8 K/min. The reaction was conducted at 453 K at an atmospheric pressure. Qualitative and quantitative analyses [34,35] of reaction products and distillates were carried out on a HP 5890-HP5971MSD and a HP 5890 gas chromatograph equipped with a flame ionization detector (FID). An OV-101 packed column was used to separate products for GC analysis. The products were mainly diphenyl oxalate, methyl phenyl oxalate, anisole (AN), and together with trace amounts of isomer products of anisole. The conversions were reported on the basis of the limiting reagent, DMO, and defined as the ratio of the moles of converted DMO to the moles of DMO fed initially to the reactor. The selectivity to MPO and DPO was defined as the moles of MPO and DPO produced per 100 mol of consumed DMO, and the yields of MPO and DPO were obtained from multiplication of DMO conversion by the selectivity to MPO and DPO.

3. Results and discussion

3.1. Surface area (S_{BET})

The specific surface areas (m^2/g) obtained for the different catalysts are shown in Table 1. The specific surface areas of supported catalysts were greater than those of pure MoO_3 and SnO_2, irrespective of Mo and Sn loading. The surface area of silica-supported Mo-Sn catalyst decreased, as expected, when the Mo and Sn loading increased from 1 to 16 wt.%. Deposit of small particles of molybdenum and stannic oxides on the walls and/or in the mouth of the smaller pores of the silica may account for decreasing the BET area.

3.2. Comparison between the catalytic behaviors of MoO_3/SiO_2, SnO_2/SiO_2, and bimetallic MoO_3-SnO_2/SiO_2

The transesterification of dimethyl oxalate was carried out at 453 K under atmospheric pressure using pure oxides, sup-

Table 1
Specific area of SiO_2, MoO_3, SnO_2, supported MoO_3, SnO_2, and bimetallic MoSn oxide catalysts

Entry	Catalysts	Sn loading (wt.%)	Mo loading (wt.%)	BET Surface (m^2/g)
A_1	SiO_2	–	–	231
A_2	MoO_3	–	–	3
A_3	SnO_2	–	–	8
B_1	MoO_3/SiO_2	–	8	129
B_2	SnO_2/SiO_2	8	–	176
C_1	MoO_3-SnO_2/SiO_2	1	1	190
C_2	MoO_3-SnO_2/SiO_2	2	2	174
C_3	MoO_3-SnO_2/SiO_2	4	4	171
C_4	MoO_3-SnO_2/SiO_2	6	6	152
C_5	MoO_3-SnO_2/SiO_2	8	8	144
C_6	MoO_3-SnO_2/SiO_2	10	10	102
C_7	MoO_3-SnO_2/SiO_2	12	12	102
C_8	MoO_3-SnO_2/SiO_2	14	14	100
C_9	MoO_3-SnO_2/SiO_2	16	16	78

Table 2
Catalytic activity of oxides, supported monometallic oxide, and supported bimetallic MoSn oxide catalysts[a]

Catalysts	Conversion (%)[b]	Selectivity (%)			Yield (%)	
		AN	MPO	DPO	MPO	DPO
A_1	1.7	0	100.0	0	1.7	0
A_2[c]	54.1	2.1	42.7	13.0	23.1	7.0
A_3	2.8	7.2	57.1	35.7	1.6	1.0
B_1	54.4	1.0	83.4	15.6	43.2	8.1
B_2	46.7	0.8	76.7	22.5	35.8	10.5
C_1	46.0	0.5	86.8	12.7	39.9	5.9
C_2	47.3	0.7	88.7	10.6	41.9	5.0
C_3	47.7	0.8	88.6	10.6	42.2	5.1
C_4	50.2	0.9	88.4	10.7	44.4	5.4
C_5	55.5	0.7	86.7	12.6	48.1	7.0
C_6	56.7	0.6	86.7	12.7	49.1	7.2
C_7	57.3	0.6	86.7	12.7	49.7	7.3
C_8	74.6	0.5	81.5	18.0	60.8	13.4
C_9	58.8	0.6	85.2	14.2	50.1	8.3

MPO: methyl phenyl oxalate; DPO: diphenyl oxalate; AN: anisole.
[a] Reaction conditions: catalyst, 1.8 g; phenol, 0.5 mol; *n*(PhOH)/*n*(DMO), 5.0; reaction time, 2 h; reaction temperature, 453 K.
[b] Based on DMO charged.
[c] Benzyl alcohol and methyl phenol were formed as main byproduct besides anisole.

ported bimetallic catalysts, and corresponding monometallic ones. The results of dimethyl oxalate conversion and selectivities to MPO, DPO, and AN as a function of active component for the different catalysts are shown in Table 2.

First, the catalytic behavior of supported SnO_2/SiO_2 and pure SnO_2 were compared. The activity of SnO_2/SiO_2 (DMO conversion was 46.7%, and MPO and DPO concentrations in the products were 76.7% and 22.5%, respectively.) was higher than that of pure stannic oxide (DMO conversion was 2.8%). Similar phenomenon was observed in the case of MoO_3 and MoO_3/SiO_2. It was worth pointing out that byproducts, benzyl alcohol and methyl phenol except anisole, were formed when MoO_3 was used as a catalyst. We carried out a preliminary study on the effect of different supports and a part of the results was reported elsewhere [30]. Briefly, these byproducts can be restrained effectively by using SiO_2 as a carrier.

Entries C_1–C_9 show the effect the loading amount of active component Mo and Sn on the DMO conversion and products selectivities. Increasing the Mo and Sn loadings from 1 to 14% increased the conversion of DMO from 46% to 74.6%. At mean time, the yields of MPO and DPO were increased from 39.9% and 5.9% to 60.8% and 13.4%, respectively. And thereafter decrease in DMO conversion and yields of MPO and DPO were observed. Moreover, the MPO selectivity was higher than 80% while the DPO selectivity varied from 10% to 15% dependent on the Mo and Sn loadings. Only AN was formed as a byproduct. And the total selectivities to MPO and DPO were up to 99% all along, namely, AN selectivity was lower than 1%.

3.3. Quantitative analysis by XPS

Surface atomic ratios calculated from XPS peak heights and atomic sensitivities [36] by assuming uniform distribution of all elements besides carbon are compared to the nominal atomic composition in order to obtain information on the structure of the surface and the dispersion of the active phases. The simplified formula used for the calculation of relative surface atomic compositions does not take into account inelastic mean free path effects due to the energy difference between the different peaks. The atomic sensitivities obtained from reference [36] were corrected taking into account the measured energy dependence of our analyzer transmission. In Table 3, the calculated surface atomic ratios and the mass ones, observed for each catalyst sample, are summarized.

In the case of the bimetallic MoO_3-SnO_2/SiO_2 catalysts, it can be noticed that the atomic ratios Mo:Si are lower than the corresponding ratios on the monometallic catalysts with the

Table 3
Elements content of the surface of catalysts with different Sn/Mo loading amount measured by XPS

Element	8%Mo		1%Mo-1%Sn		2%Mo-2%Sn		4%Mo-4%Sn		8%Mo-8%Sn		16%Mo-16%Sn	
	wt.%	at.%	wt.%	at.%	wt.%	at.%	wt.%	at.%	wt.%	at.%	wt.%	at.%
O	50.5	68.0	55.2	69.3	54.4	69.0	53.6	69.4	51.2	68.3	43.3	67.5
Si	38.3	29.5	42.2	30.2	41.6	30.1	39.2	29.0	38.8	29.6	29.0	25.8
Mo	11.2	2.5	1.4	0.3	2.8	0.6	5.5	1.2	7.2	1.6	17.7	4.6
Sn	–	–	1.2	0.2	1.2	0.2	1.7	0.3	2.8	0.5	10.0	2.1

same Mo loading. This interesting result indicates that the presence of the Sn promoter leads to a better dispersion of the molybdena phase. When Mo(Sn) loadings are below 2%, the Mo/Sn weight ratio is close to the nominal composition (1:1) within the experimental error of about ±10%. However, with the increase in the Mo(Sn) loading, this phenomenon was not observed, which suggests that Sn is either less dispersed than Mo or it is sandwiched between the molybdenum phase and the support.

Moreover, XPS analysis provided bond energy equal to 487.4 ± 0.2 eV referring to $Sn3d_{5/2}$, which is characteristic of Sn(IV). The Sn^{4+} peak of 487.4 eV represented SnO_2 due to dibutyltin dilaurate (DBTDL) as the Sn precursor (Eq. (5)). The analogous deduction is also applicable to the case of Mo (232.4 ± 0.2 eV referring to $Mo3d_{5/2}$) (Eq. (6)).

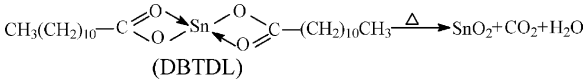

(DBTDL) (5)

$$(NH_4)_6Mo_7O_{24} \cdot 4H_2O \xrightarrow{\Delta} 7MoO_3 + 6NH_3 + 7H_2O \quad (6)$$

3.4. X-ray diffraction (XRD)

The X-ray powder diffraction analysis was undertaken to determine the composition and crystallinity of Mo or Sn species in Mo-Sn catalysts. The XRD patterns of supported bimetallic MoO_3-SnO_2/SiO_2 catalysts and corresponding monometallic MoO_3/SiO_2 and SnO_2/SiO_2 are given in Fig. 1. The X-ray diffractograms only showed the crystalline phases corresponding to SnO_2 (JCPDS 41-1445) and MoO_3 (JCPDS 35-0609). No additional XRD peak was observed, indicating the absence of definite Sn-Mo mixed oxide compounds. It was shown that there were no characteristic diffraction peaks of Mo species ($d = 0.327$, 0.381, and 0.347 nm) when the loading amount of Mo was less than 2%. However, when the Mo loading increased beyond a borderline, i.e. above its dispersion capacity, the marked change in intensity or offset of peak position can be detected at high loadings, which indicated that Mo(VI) species was dispersed in the form of an amorphism at low Mo loading and that MoO_3 with the orthorhombic crystal structure appeared at higher loading.

Also, the intensity ratio of the SnO_2:MoO_3 peaks and crystallinity of MoO_3 and SnO_2 increased with the increase in Mo(Sn) loadings, accompanied by enhancement of the DMO conversion. The changes exhibited by supported binary oxides indicated the appearance of tetragonal crystal SnO_2 phase strengthened the promotional effect of Sn and led to the increase in the activity of supported bimetallic MoO_3-SnO_2/SiO_2 catalysts.

3.5. IR characterization of adsorbed pyridine

FT-IR analysis of adsorbed pyridine allows a clear distinction between Brönsted and Lewis acid sites. IR band at 1455 cm^{-1} is attributed to pyridine adsorbed on

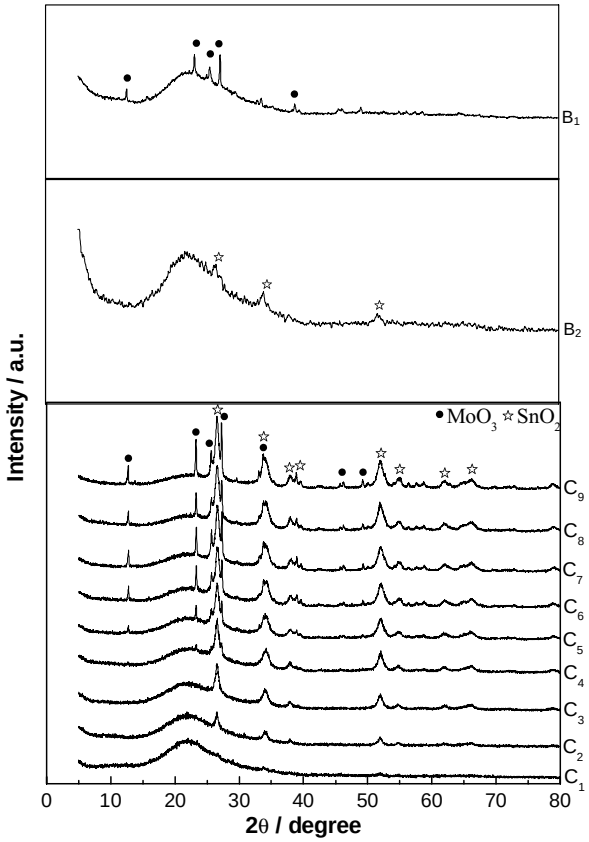

Fig. 1. XRD spectra of supported monometallic oxide and supported bimetallic MoSn oxide catalysts with different Sn/Mo loadings.

Lewis acid sites, IR band at 1545 cm^{-1} to that adsorbed on Brönsted acid sites. While the peak at 1490 cm^{-1} can be ascribed to the overlapping of Brönsted acid and Lewis acid sites [37–39]. From Fig. 2, it can be seen that IR pyridine adsorption spectra of supported bimetallic MoO_3-SnO_2/SiO_2 catalysts and the corresponding monometallic ones (MoO_3/SiO_2, SnO_2/SiO_2) have peaks

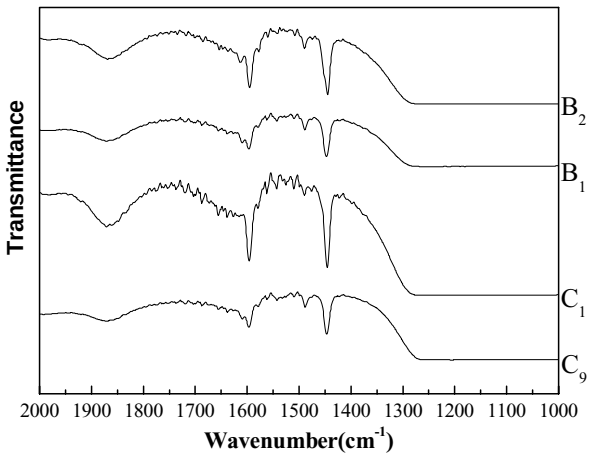

Fig. 2. FT-IR spectrum absorbed pyridine of supported bimetallic MoO_3-SnO_2/SiO_2 catalysts and corresponding monometallic ones.

at 1455 cm^{-1} and 1490 cm^{-1}, while the peak at 1545 cm^{-1} is absent. This means that there are only Lewis acid sites, but not Brönsted acid sites on these catalysts. From the intensity of the peaks in Fig. 2, the relative acid amount of bimetallic MoO_3-SnO_2/SiO_2 catalysts and corresponding monometallic ones can be deduced. We found that MoO_3-SnO_2/SiO_2 catalyst with 1% Mo(Sn) loadings had the largest acid amount. From the XRD analysis above, we recognized that Mo atom on the surface was mantled when the amount of Sn loading was higher than 2%, which reduced the Lewis acid center on the catalyst surface. So, the relative acid amount of MoO_3-SnO_2/SiO_2 catalysts decreased with increasing Mo(Sn) loading from 1 to 16%.

3.6. Temperature-programmed desorption of ammonia (NH_3-TPD) analysis

NH_3-TPD characterization was conducted to survey the acid strength of MoO_3-SnO_2/SiO_2 catalysts and the influence of Mo(Sn) loadings on it. In the NH_3-TPD curves, peaks are generally distributed into two regions: below and above 673 K referred to as low-temperature (LT) and high-temperature (HT) regions, respectively. The peaks in the HT region can be attributed to the desorption of NH_3 from strong Brönsted and Lewis type acid sites, and the peaks in the LT region is assigned as the desorption of NH_3 from weak acid sites [40,41]. From the result shown in Fig. 3, it can be seen that the peaks only appeared in the low temperature region, confirming that there only existed weak acid sites on the surface of MoO_3-SnO_2/SiO_2 catalysts with Mo(Sn) loading ranging from 1 to 16%. Furthermore, the maximum temperature offset is 20 K. This indicates that the amount of Mo(Sn) loading has little effect on the strength of the surface acid on MoO_3-SnO_2/SiO_2 catalysts. We carried out a preliminary study on the effect of acid strength on the selectivity to anisole and a part of the results was reported elsewhere [13]. Briefly, the weak acid sites are responsible for the formation of MPO, while the strong acid sites were in favor of the formation of anisole. Therefore, the results of TPD gave the reason for high selectivity to MPO and DPO over silica-supported MoO_3-SnO_2 catalysts.

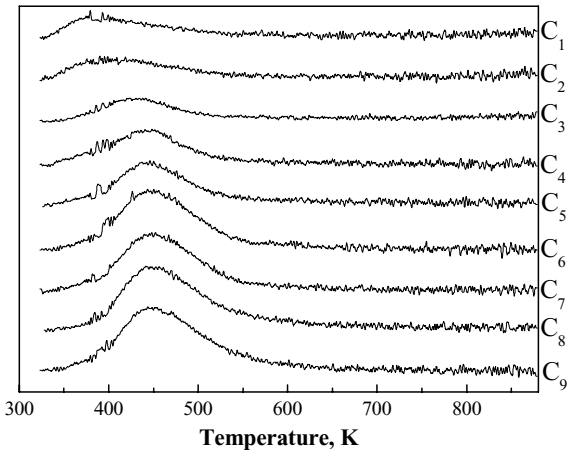

Fig. 3. NH_3-TPD spectrum of supported bimetallic MoO_3-SnO_2/SiO_2 catalysts.

Furthermore, it is pointed out that the catalytic performance, especially DMO conversion, was not directly related with the amount of surface acid. There may be two reasons. The acid sites can be detected by NH_3 with small molecule volume. But for transesterification reaction, because the molecular size of DMO and phenol was too large to access the pore of SiO_2 freely, not all acid centers turned out to be effective active sites. On the other hand, the promotional effect of Sn offset the decrease in acid amount with increasing Mo(Sn) loading. This integrated effect enhanced the catalytic activity of MoO_3-SnO_2/SiO_2.

4. Conclusions

From the studies on the transesterification of DMO with phenol over MoO_3-SnO_2/SiO_2 catalysts, the following conclusions could be derived. The catalysts of MoO_3-SnO_2/SiO_2 exhibited excellent catalytic performance. Under the experimental conditions, the Mo(Sn) loading 14% in weight gave 74.6% conversion of DMO and 99.5% selectivity to the target products, MPO and DPO. Mo(VI) species was dispersed in the form of an amorphism at low Mo loadings and MoO_3 with the orthorhombic crystal structure appeared at high loadings. The interdispersion between MoO_3 and SnO_2 played an important role in modifying the catalytic behavior. Only Lewis weak acids were present on catalyst surface and the amount of Mo(Sn) loading had little effect on the strength of the surface acid. The integrated effect between the weak Lewis acid sites and the promotional effect of Sn was related with the catalytic activity of transesterification of DMO with phenol.

Acknowledgements

The authors wish to acknowledge National Natural Science Foundation (NSFC) of China (No.20276050) and Tianjin Science and Technology Committee (TSTC) of China (No.033103511) for financial aid.

References

[1] S.K. Sikdar, CHEMTECH 112 (February 1987).
[2] U. Curtius, L. Bottoenbruch, H. Schnell, US Patent 3,442,854 (1969).
[3] H. Yamana, T. Kuni, T. Furusawa, H. Nakai, Y. Hiro, US Patent 3,888,826 (1975).
[4] D. Brunelle, US Patent 4,321,356 (1982).
[5] J.B. Starr, A. Ko, US Patent 4,383,092 (1983).
[6] A.G. Shaikh, S. Sivaram, Chem. Rev. 96 (1996) 951.
[7] J. Beranek, J. Hlavackova, Nucleic Acid Chem. 2 (1978) 999.
[8] H. Yoshinori, K. Hideki, H. Michio, JP Patent 0,900,923 (1997).

[9] Y. Ono, Appl. Catal., A 155 (1997) 133.
[10] Y. Ono, Pure Appl. Chem. 68 (1996) 367.
[11] K.J.L. Linsen, J. Libens, P.A. Jacobs, Chem. Commun. 22 (2002) 2728.
[12] W.B. Kim, J.S. Lee, J. Catal. 185 (1999) 307.
[13] X. B Ma, H.L. Guo, S.P. Wang, Fuel Process Technol. 83 (2003) 275.
[14] X.B. Ma, J.L. Gong, S.P. Wang, Catal. Commun. 5 (2004) 101.
[15] K. Okuyama, J. Sugiyama, R. Nagahata, M. Asai, M. Ueda, K. Takeuchi, J. Mol. Catal., A 203 (2003) 21.
[16] H. Ishii, M. Goyal, M. Ueda, K. Takeuchi, M. Asai, Appl. Catal., A 201 (2000) 101.
[17] H. Musso, Angew. Chem. Int. Ed. 2 (1963) 7.
[18] F.M. Mei, G.X. Li, J. Nie, H.B. Xu, J. Mol. Catal., A 184 (2002) 465.
[19] K. Nishihira, S. Tanaka, K. Harada, R. Sugise, US Patent 5,834,615 (1997).
[20] K. Nishihira, S. Tanaka, K. Harada, R. Sugise, A. Shiotani, K. Washio, US Patent 5,922,827 (1999).
[21] T. Matsuzaki, A. Nakamura, Catal. Surv. Jpn. 1 (1997) 77.
[22] K. Nishihira, S. Tanaka, Y. Nishida, I. Hirofumi, S. Fujitsu K. Harada, R. Sugise, US Patent 5,811,573 (1998).
[23] S.P. Wang, X.B. Ma, H.L. Guo, J.L. Gong, J. Mol. Catal., A 214 (2004) 273.
[24] M.S. Wainwright, N.R. Foster, Catal. Rev. Sci. Eng. 19 (1979) 211.
[25] F. Cavalli, F. Cavani, I. Maneti, F. Trifiro, Catal. Today 1 (1987) 245.
[26] C.R. Dias, M.F. Portela, G.C. Bond, J. Catal. 157 (1995) 344.
[27] K.V.R. Chary, G. Kishan, T. Bhaskar, J. Phys. Chem. 102 (1998) 6792.
[28] A.N. Startsev, Catal. Rev. Sci. Eng. 37 (1995) 353, and references therein..
[29] L.T. Weng, B. Delmon, Appl. Catal., A 81 (1992) 141.
[30] J.L. Gong, X.B. Ma, S.P. Wang, J. Mol. Catal., A 207 (2004) 215.
[31] I. Halasz, A. Brenner, M. Shelef, K. Ng, Appl. Catal., A 82 (1992) 51.
[32] J.L. Gong, X.B. Ma, X. Yang, Catal. Commun. 5 (2004) 179.
[33] J. Foschiera, T. Pizzolato, E. Benvenutti, J. Braz. Chem. Soc. 12 (2001) 159.
[34] S.P. Wang, Z.H. Li, X.B. Ma, G.H. Xu, Chin. J. Anal. Chem. 30 (2002) 829.
[35] S.P. Wang, X.B. Ma, Z.H. Li, G.H. Xu, Chin. J. Anal. Chem. 30 (2002) 1085.
[36] D. Briggs, M.P. Seah (Eds.), Practical Surface Analysis, vol.1, 2nd ed., Wiley, New York, 1990, p. 201.
[37] T. Barzetti, E. Selli, D. Moscotti, L. Forni, J. Chem. Soc., Faraday Trans. 92 (1996) 1401.
[38] T.R. Hughes, H.M. White, J. Phys. Chem. 71 (1967) 2192.
[39] C.A. Emeis, J. Catal. 141 (1993) 347.
[40] F. Lónyi, J. Valyon, Microporous Mesoporous Mater. 47 (2001) 293.
[41] M. Sawa, M. Niwa, Y. Murakami, Zeolites 10 (1990) 532.